

Examinations of Convective Processes Representations and Inertial Stability in a Tropical Cyclone Model

Jong-Jin Baik and Seung-Man Lee

Global Environment Laboratory and Department of Astronomy and Atmospheric Sciences, Yonsei University, Seoul, Korea

Chun-Ho Cho

Numerical Weather Prediction Division, Korea Meteorological Administration, Seoul, Korea

(Manuscript received 8 June 1993)

태풍 모형에서의 대류 과정 표현과 관성 안정도에 관한 조사

백종진 · 이승만

연세대학교 지구환경연구소 및 천문대기과학과

조천호

기상청 수치예보과

(1993년 6월 8일 접수)

요약

축대칭 태풍 모형을 이용하여 각각 다른 대류 과정 표현 방법들이 태풍의 발달에 미치는 영향과 태풍이 급속히 발달하는 동안 관성 안정도의 역할을 조사하였다. 암시적 방법(적운 모수화)과 명시적 방법을 함께 사용하는 실용주의적 방법은 명시적 방법만을 사용할 때보다 잇점을 가지는데 이는 조건부·불안정하고 불포화된 대기에서는 암시적 방법을 첨가함으로써 잠열 방출, 강수 및 해면 기압 하강이 명시적 방법을 사용할 때보다 일찍 시작되기 때문이다. 실용주의적 방법은 암시적 방법과 격자 규모 과포화를 제거하는 간단한 방법을 사용하는 전통적 방법보다 격자 규모 상변화 과정을 더욱 정확하게 취급할 수 있다. 그러나 실용주의적 및 전통적 방법들은 분해되지 않는(암시적) 구름과 분해되는(명시적) 구름이 깊은 충을 통하여 같은 수평 격자점에 공존할 때 개념적인 문제점을 내포하고 있다. 이 문제점은 태풍의 진화 기간 동안 암시적 및 명시적 방법이 각각 상당한 양의 잠열을 발생시킬 때 일어난다. 비록 모형 태풍의 진화는 다소 대류 과정 취급에 민감하지만 태풍의 최종 강도는 상호간 많이 다르지가 않다.

모형 태풍이 급속히 발달하는 동안 가장 관성적으로 안정한 지역은 하층 대류권에서 접선 방향 풍속과 접선 방향 풍속의 방사상 기울기가 큰 최고 풍속 지점의 바로 안쪽에 위치한다. 이 지역은 관성적으로 더 안정해지며 안쪽으로 움직인다. 강제 이차 순환에 대한 단순화된 진단 방정식을 사용한 Schubert와 Hack(1982)의 이론적 연구와 본 수치 모형 모사를 기초하여 관성 안정도 증가와 대기를 따뜻하게 하는 열 효율 증가 사이의 비선형적 양의 되먹임(nonlinear positive feedback)은 태풍의 급속한 발달에 중요한 역할을 한다는 것을 강조하였다.

Abstract

An axisymmetric tropical cyclone model is used to investigate the impacts of including different convective processes representations on the storm development and the roles of inertial stability

during the rapid intensification of the storm. The pragmatic approach with both the implicit (cumulus parameterization) and explicit methods has an advantage over the explicit method, because in the conditionally unstable and subsaturated atmosphere the addition of the implicit method begins latent heat release, precipitation and surface pressure drops earlier than the explicit method alone. The pragmatic approach can treat grid-scale phase change processes more accurately than the traditional approach with the implicit method and simple method of removing grid-scale supersaturation. However, the pragmatic and traditional approaches provide a conceptual problem when unresolved (implicit) and resolved (explicit) clouds coexist at the same horizontal grid location through a deep layer. This occurs during the storm evolution period when each of the implicit and explicit methods can produce a significant amount of latent heating. Although the model storm evolution is somewhat sensitive to the treatment of convective processes, final storm intensities are not significantly different from each other.

During the rapid intensification of the model storm, the most inertially stable region is located just inside the radius of the maximum wind in the lower troposphere, where both the tangential wind speed and the radial gradient of the tangential wind speed are large. This region becomes much more inertially stable and moves inward. Based on the theoretical work using a simplified diagnostic equation for the forced secondary circulation by Schubert and Hack (1982) and the present numerical model simulation, it is emphasized that a nonlinear positive feedback between the increasing inertial stability and the increasing heating efficiency to warm the atmosphere can play an important role in the rapid intensification of the storm.

1. Introduction

Since the primary energy source to drive tropical cyclones comes from the latent heat release by cumulus convection through energy supply by vortex-ocean interaction, a proper substitute for the observed cumulus clouds is required for a tropical cyclone model. Early attempts (e.g., Kasahara, 1961) to numerically simulate tropical cyclone development were unable to explain the cyclone-scale circulation because the fastest growth of disturbances occurred on the smallest horizontal scale resolved by the model. The mathematical theory proposed by Ooyama (1964) and Charney and Eliassen (1964) overcame this problem by combining the cumulus scale and the cyclone-scale in a cooperative way. Stimulated by their pioneering work, much efforts have been made to simulate tropical cyclone development using numerical models with subgrid-scale cumulus convective processes related to the grid-scale variables with some closure assumptions, that is, with cumulus parameterizations [see Table 4.1. in Anthes (1982) for summary].

Contrary to the research direction of parameterizing cumulus convection in tropical cyclone models, Yamasaki (1977) first attempted to simulate a tropical cyclone using an axisymmetric nonhydrostatic model

with cumulus convection explicitly resolved on a horizontal resolution of 0.4 km near the storm center. Rosenthal (1978) also treated cumulus convection explicitly in his axisymmetric hydrostatic tropical cyclone model with a 20 km horizontal resolution. Following their research line, some investigators avoided cumulus parameterization by adopting explicit approach in either hydrostatic (e.g., Jones, 1980) or nonhydrostatic (e.g., Rotunno and Emanuel, 1987) tropical cyclone models.

Because the horizontal scale of convective elements is on the order of 0.1-1 km, one can, in principle, make a choice between implicit and explicit approaches depending on the horizontal model resolution. However, some previous studies (e.g., Rosenthal, 1978) imply that the explicit approach can be used in a nearly saturated environment with a large grid-scale forcing such as an eyewall even if the horizontal grid size is larger than the horizontal scale of convective elements. Also, a review of previous studies indicates that there is some range of horizontal model resolution over which either implicit or explicit approach can simulate tropical cyclones well [e.g., 15 km resolution with the Arakawa-Schubert cumulus parameterization in Hack and Schubert (1980); 15 km resolution with the explicit approach in Rotunno and Emanuel (1987); 20 km resolution near the storm center with the convective adjustment scheme in Kurihara (1975); 20 km resolution with the explicit

approach in Rosenthal (1978)].

In models employing cumulus parameterizations, the grid-scale supersaturation is usually removed by assuming that either all of the condensed water vapor resulting from supersaturation at a level immediately falls out as rain or falls into the next lower level and evaporates depending on the degree of relative humidity at that level. Using an axisymmetric tropical cyclone model with a 20 km horizontal resolution, Baik *et al.* (1991b) showed that the parameterized latent heating is dominant at the early stage of the storm development and the grid-scale latent heating is dominant at the mature stage, and that the storm evolution is sensitive to the treatment of the evaporation of liquid water in the grid-scale condensation scheme. These results imply that it is preferable to include a liquid water prediction equation when simulating tropical cyclones with a model resolution fine enough for grid-scale heating to be important so that grid-scale phase change processes can be treated more accurately.

As an extension of our previous work, the impacts of including different convective processes representations in an axisymmetric hydrostatic tropical cyclone model are investigated. Especially, we will emphasize advantages and a conceptual problem when both parameterized subgrid-scale convection and explicit schemes are included. Although the research of testing and evaluating cumulus parameterizations and/or explicit method has been extensively performed in midlatitude convective systems and extratropical cyclones during the past decade (e.g., Zhang, 1988) and an individual cumulus parameterization scheme, once developed, has been usually tested and evaluated using an idealized axisymmetric tropical cyclone model (e.g., Anthes, 1977), a comparative study of different convective processes representations in a tropical cyclone model still needs to be investigated to help better represent convective processes in research and operational tropical cyclone models. This is the first objective of present study.

In nature, tropical cyclones typically develop slowly until reaching a certain threshold and then intensify much more rapidly. The rapid intensification can be evaluated in terms of the rate of decrease in central surface pressure or the rate of increase in maximum wind speed. Holliday and Thompson

(1979) analyzed 305 tropical cyclones in the northwest Pacific for a 21 year period and found that the mean of the maximum 24 h deepening rate is 29.7 hPa/d. 79 typhoons (26% of the sample) had deepening rates greater than 42 hPa/d. This deepening rate was used to identify rapidly intensifying typhoons.

A number of studies have suggested mechanisms which affect tropical cyclone intensification. Schubert and Hack (1982) analytically solved the diagnostic equation for the forced secondary circulation under the assumptions of constant static stability, non-baroclinicity and barotropic vortex profile and investigated the effects of inertial stability on tropical cyclone development. They showed that the nonlinear feedback process between increasing inertial stability and increasing heating efficiency has a major influence on tropical cyclone development. Using an axisymmetric tropical cyclone model, Willoughby *et al.* (1984) examined the symmetric instability in the upper troposphere and proposed that it may induce either vortex-scale ascent or formation of convective rings, but both processes, once initiated, can reduce the instability by the entrainment of air into the outflow region from the inertially stable lower troposphere. Weatherford (1987) examined typhoon structural evolution in the inner core region ($0\text{--}1^\circ$ radius) and outer core region ($1\text{--}2.5^\circ$ radius) with the composited aircraft reconnaissance data at 700 hPa in the northwest Pacific for a 5 year period and speculated that as the outer core circulation builds up and correspondingly the inertial stability increases, the intensification of the inner core slows down. We investigate possible roles of inertial stability in a rapidly intensifying tropical cyclone through numerical model simulation. This is the second objective of present study.

In section 2, the axisymmetric tropical cyclone model used in this study and three different methods of representing convective processes are described. In section 3, results of numerical simulations are presented. Conclusions are given in section 4.

2. Model Description and Convective Processes Representations

The numerical model used in this study is the

axisymmetric, primitive equation, hydrostatic, finite-difference model described in Baik *et al.* (1990a). The model includes the conservation equations for momentum, mass, energy and water vapor and the equation of state. The governing equation set is derived on an f-plane with axisymmetric polar coordinates in the horizontal and σ -coordinate in the vertical, which is defined by $\sigma = (p - p_t)/(p_s - p_t)$. Here, p is the pressure, p_t the pressure at the model top (specified as 50 hPa) and p_s the surface pressure. The model has 15 vertical layers with nonuniform thickness and a uniform horizontal resolution of 20 km on a horizontal domain size of 1000 km. Table 1 shows the 15 σ levels and the corresponding pressure levels for the initial surface pressure at the model lateral boundary. The spectral radiation boundary condition (Hack and Schubert, 1981), which uses a different gravity wave speed for each vertical mode, is implemented into the model to minimize gravity wave reflection at the lateral boundary. The time step is 30 sec. The model contains subgrid-scale horizontal and vertical diffusion, air-sea interaction, dry convective adjustment and moist convective processes. The radiation physics is not employed in this study.

The initial wind field consists of tangential wind and zero radial wind. The structure of the initial tangential wind is

$$v = v_m \left[\frac{2(r/r_m)}{1+(r/r_m)^2} \right] \left[\frac{3(\sigma/\sigma_m)}{2+(\sigma/\sigma_m)^3} \right] \quad (1)$$

where v is the tangential wind speed and r the radius in polar coordinates. The maximum tangential wind speed v_m , the radius of the maximum wind r_m and the σ level of the maximum wind σ_m are specified as 10 m/s, 210 km and 0.9, respectively. The initial temperature and surface pressure distributions inside the lateral boundary are determined using the hydrostatic and gradient wind equations with the temperature profile obtained from the mean tropical clear areas sounding in the western Pacific (Gray *et al.*, 1975) and a surface pressure of 1008.7 hPa at the lateral boundary. The initial moisture field is taken from the mean tropical cluster environment sounding in the western Pacific (Gray *et al.*, 1975). To reduce the integration time before the storm develops, a Gaussian-type perturbation with the amplitude of 10% in relative humidity and e-folding radius of 200 km is added to the initial moisture field near the storm center. The Coriolis parameter is evaluated at 20°N and the sea surface temperature is set to 28°C. For further details of the numerical model, see Baik *et al.* (1990a). In the following subsections, three different methods for treating convective processes are described.

2.1 Cumulus Parameterization and Simple Method of Removing Grid-scale Supersaturation

In the first method, both subgrid-scale cumulus parameterization (implicit method) and simple method of removing grid-scale supersaturation are included. The convective adjustment scheme proposed by Betts (1986) is used to parameterize precipitating deep cumulus convection. Nonprecipitating shallow convection is not included. The convective adjustment scheme is based on the concept that in the presence of convection the local thermodynamic structures are constrained by convection and adjusted towards an observed quasi-equilibrium reference state. The subgrid-scale convective heating and moistening terms are represented by

$$F_T = \frac{T_{ref} - \bar{T}}{\tau} \quad (2)$$

Table 1. The σ levels and the corresponding pressure levels assuming that $p_s = 1008.7$ hPa.

| level index | σ | pressure (hPa) |
|-------------|----------|----------------|
| 1 | 0.0209 | 70 |
| 2 | 0.0522 | 100 |
| 3 | 0.1043 | 150 |
| 4 | 0.1565 | 200 |
| 5 | 0.2086 | 250 |
| 6 | 0.2608 | 300 |
| 7 | 0.3651 | 400 |
| 8 | 0.4694 | 500 |
| 9 | 0.5737 | 600 |
| 10 | 0.6780 | 700 |
| 11 | 0.7823 | 800 |
| 12 | 0.8345 | 850 |
| 13 | 0.8866 | 900 |
| 14 | 0.9482 | 960 |
| 15 | 0.9805 | 990 |

$$F_q = \frac{q_{vref} - \bar{q}_v}{\tau} \quad (3)$$

respectively. Here, T is the temperature, q_v the water vapor mixing ratio and τ the adjustment (or relaxation) time scale. The subscript *ref* denotes the reference state and the overbar the grid point value before convection. The essence of the scheme is to construct the reference thermodynamic profiles. The deep convection scheme considers the observational evidence that in the presence of penetrative deep convection a quasi-equilibrium temperature profile below the freezing level closely follows a moist virtual adiabat, which includes buoyancy correction due to cloud water. For the numerical simulation, the adjustment time scale and the saturation pressure departure at the lowest model level are specified as 0.5 h and -30 hPa, respectively. The stability weight on the moist adiabat in the lower atmosphere is internally computed by assuming that the reference temperature profile is exactly equal to that on a moist virtual adiabat (Baik *et al.*, 1991b). For further details of the convective adjustment scheme, the reader is referred to Betts (1986) and Baik *et al.* (1990a).

When the atmosphere is found to be supersaturated at a grid point, the excess water vapor is condensed to liquid water and grid-scale latent heat is released. This process can be expressed by

$$q'_v = q_v - \Delta C \quad (4)$$

$$T' = T + \frac{L}{c_p} \Delta C \quad (5)$$

where q'_v and T' are the adjusted water vapor mixing ratio and temperature, respectively, after the grid-scale phase change processes. The ΔC is the condensation amount during the time step, L the latent heat of condensation and c_p the specific heat at constant pressure. The resultant liquid water is assumed to immediately fall out as rain. The q'_v is the saturation mixing ratio at T' , that is,

$$q'_v = q_{vs}(T', p) = \frac{\epsilon e_s(T')}{p - e_s(T')} \quad (6)$$

Here, ϵ is 0.622 and $e_s(T')$ is the saturation water vapor pressure at T' , which is calculated using the Tetens' formula. From (4), (5) and (6), it follows that

The above nonlinear equation in the unknown T' is

$$[(\epsilon + q_v) \frac{L}{c_p} + T - T'] e_s(T') + p T' - (\frac{L}{c_p} q_v + T) p = 0 \quad (7)$$

numerically solved using the Newton's iteration method. Then, ΔC and q'_v are computed from (5) and (4).

2.2 Explicit Method

In the second method, a prognostic equation for liquid water is incorporated to explicitly resolve convective processes. The effect of the subgrid-scale convection is not included. The continuity equation for liquid water mixing ratio q_l can be written as where $\pi = p_s - p_t$, t is the time, u the radial wind speed

$$\frac{\partial}{\partial t}(\pi r q_l) = -\frac{\partial}{\partial r}(\pi r u q_l) - \frac{\partial}{\partial \sigma}(\pi r \dot{\sigma} q_l) + \pi r D_{q_l} + \pi r M_{q_l} \quad (8)$$

and σ the vertical σ -velocity. The diffusion term D_{q_l} is parameterized according to the method of Baik *et al.* (1990a). The microphysical process terms due to the phase changes of water substance, which are added to the thermodynamic energy equation (M_T), the continuity equation for water vapor (M_{q_v}) and the continuity equation for liquid water (M_{q_l}), are represented by

where dq_{vs}/dt is the condensation / evaporation rate, ρ

$$M_T = -\frac{L}{c_p} \frac{dq_{vs}}{dt} \quad (9)$$

$$M_{q_v} = \frac{dq_{vs}}{dt} \quad (10)$$

$$M_{q_l} = -\frac{dq_{vs}}{dt} + \frac{1}{\rho} \frac{\partial}{\partial z}(\rho V_T q_l) \quad (11)$$

the air density, z the height and V_T the terminal velocity of liquid water. As in Rotunno and Emanuel (1987), only one class of liquid water is considered and cloud water is distinguished from rain water only through the determination of the terminal velocity of liquid water. If $q_l \leq 1$ g/kg, V_T is set to zero. If $q_l > 1$ g/kg, the following formula is used (Liu and Orville, 1969; Seitter, 1986).

where V_T is in m/s and q_l in g/kg. The condensation/

$$V_T = 5.32(q_l - 1)^{0.2} \quad (12)$$

where V_T is in m/s and q_l in g/kg. The condensation/evaporation rate is computed as follows. When the atmosphere is supersaturated at a grid point after marching one time step, the excess water vapor is condensed and grid-scale latent heat release follows. The calculation procedure is the same as that described in the simple method of removing grid-scale supersaturation (subsection 2.1). A difference is that the condensed water vapor is added to the liquid water prediction equation. When the atmosphere is subsaturated, the liquid water is completely exhausted for evaporation or the liquid water is evaporated until saturation occurs, whichever takes place first (Rotunno and Emanuel, 1987). A simple hydrostatic water loading effect is incorporated into the hydrostatic equation to include the effects of liquid water on buoyancy (Molinari and Dudek, 1986).

2.3 Cumulus Parameterization and Explicit Method

In the third method, both the implicit method (cumulus parameterization) and explicit method (subsection 2.2) described above are included.

3. Results and Discussion

3.1 Convective Processes Representations

In this subsection on convective processes representations, the numerical simulations using the methods described in subsections 2.1, 2.2 and 2.3 will be denoted by A20, B20 and C20, respectively. Figure 1 shows the time evolution of the minimum surface pressure for the numerical experiments that employ the cumulus parameterization and simple method of removing grid-scale supersaturation, the explicit method, and the cumulus parameterization and explicit method. The storm in the A20 simulation develops slowly during the first 3 days and intensifies rapidly during the next 2 days. Afterwards, the storm reaches a quasi-steady state with an average minimum surface pressure of 915 hPa.

To examine the partition of the total latent heating due to convective processes into the parameterized

subgrid-scale and grid-scale heating, Baik *et al.* (1990a and 1991b) analyzed the domain-averaged total, subgrid-scale and grid-scale precipitation rates. Results indicated that during the early development of the storm the diabatic heating comes from the parameterized cumulus convection, while at the mature stage it is mainly from the grid-scale phase change processes. In addition, the interaction between the parameterized and grid-scale heating was shown to be crucial for understanding the model storm intensification. These results also apply to the A20 simulation.

The time evolution of the minimum surface pressure in the B20 simulation (Fig. 1) indicates that the development of a tropical cyclone can be modeled in a hydrostatic model with the simple explicit microphysics. Compared with the A20 simulation, the B20 simulation exhibits a little oscillatory behavior in the time evolution of the minimum surface pressure. An examination of the grid-scale latent heating field with time in the B20 simulation reveals that regions with very large cooling rates are occasionally observed. As mentioned in Rotunno and Emanuel (1987), this might be related to the exaggerated evaporation rate for falling rain, hence exaggerated

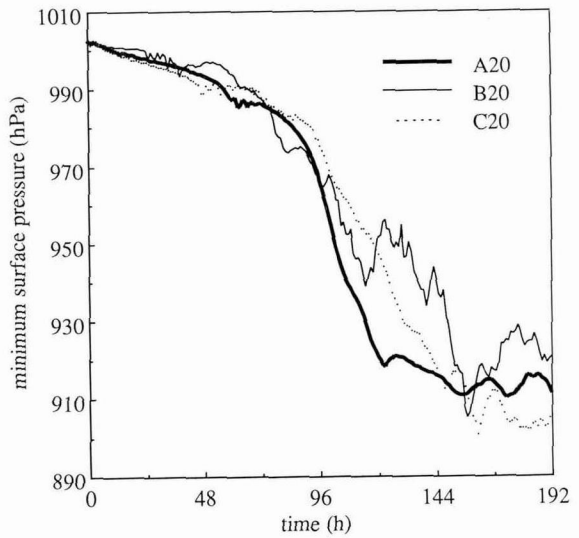


Fig. 1. The time evolution of the minimum surface pressure for the experiments with the cumulus parameterization and simple method of removing grid-scale supersaturation (A20), the explicit method (B20) and the cumulus parameterization and explicit method (C20).

cooling rate, in the present formulation of the microphysical processes.

When the cumulus parameterization is included in the B20 simulation, the model storm (C20 case) undergoes a smoother evolution during the rapidly intensifying stage than the storm in the B20 simulation. A closer examination of Fig. 1 indicates that during the first 2.5 days, the minimum surface pressure in the A20 and C20 simulations is slightly lower than that in the B20 simulation except for near 38 h. This is because in the B20 simulation the latent heat is not released until the model atmosphere first becomes supersaturated, while in the A20 and C20 simulations the parameterized latent heat is released when the vertically integrated subgrid-scale heating rate is positive in the conditionally unstable and subsaturated atmosphere during that period.

Figure 2 shows the vertical profile of the total latent heating at the radius of the maximum total heating at 192 h for the A20 simulation. Since the parameterized heating is zero at this location and time, the total heating is equal to the grid-scale heating. The maximum heating zone is located around mid-level.

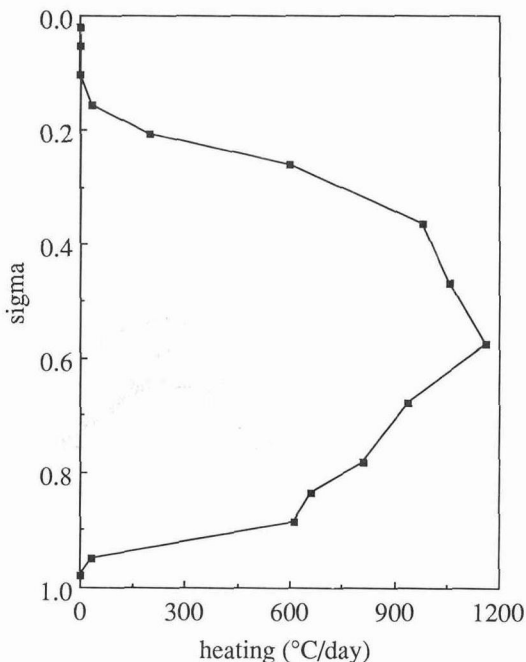


Fig. 2. Vertical total latent heating profile at the radius of the maximum total heating at 192 h for the A20 experiment.

The dominance of the grid-scale latent heating over the subgrid-scale heating at the mature stage of the simulated tropical cyclone in the A20 simulation is due to the very strong latent heat release that removes convectively unstable layers and neutralizes or stabilizes the model atmosphere, thus preventing subgrid-scale cumulus convection.

Figure 3 shows the vertical profiles of the parameterized subgrid-scale heating and grid-scale heating at a radius of 210 km at 72 h for the C20 simulation. This time is very close to the beginning of the rapid intensification of the model storm. In both the profiles, the heating occurs through deep layers and the maximum heating is found around mid-level. This figure indicates that each of the cumulus parameterization and explicit method produces a significant amount of latent heating necessary for the subsequent storm intensification. The time evolution field of the latent heating in the C20 simulation (not shown) reveals that the behavior of the partition of the total heating into the parameterized and grid-scale heating is similar to that in the A20 simulation and

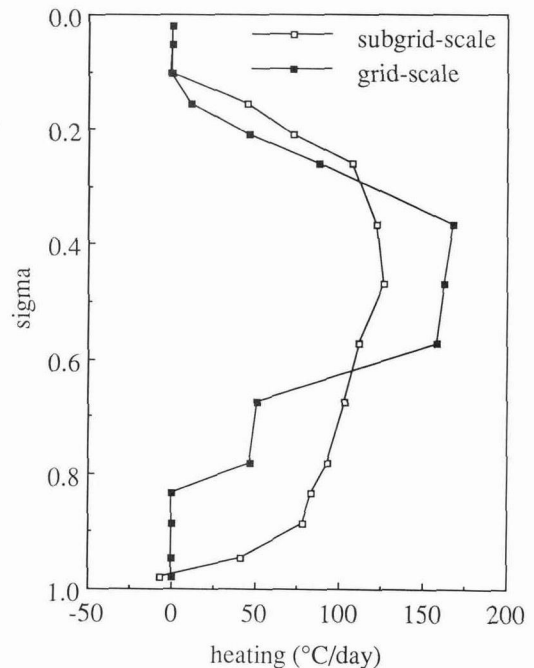


Fig. 3. Vertical profiles of the parameterized subgrid-scale latent heating and grid-scale latent heating at 210 km radius at 72 h for the C20 experiment.

exaggerated grid-scale cooling is also occasionally observed as in the B20 simulation.

During the early stage of the storm development when the model atmosphere is conditionally unstable and subsaturated near the vortex, the approach with the cumulus parameterization and explicit method simultaneously incorporated (C20 case) has an advantage over the one with the explicit method (B20 case). This is because the addition of the implicit method begins the precipitation, latent heat release and surface pressure falls earlier than the explicit method alone, in which the latent heat is not released until the model atmosphere first becomes supersaturated. However, this does not mean that understanding of tropical cyclone formation in numerical models can be well accomplished by parameterizing subgrid-scale cumulus convection, because scale separation requirements between subgrid-scale convection and grid-scale motions may not be satisfied under weak local rotational constraints (Ooyama, 1982). The approach with the cumulus parameterization and explicit method has an advantage over the one with the cumulus parameterization and simple method of removing grid-scale supersaturation (A20 case) in that it can treat grid-scale phase change processes more accurately.

However, the approach in the C20 (also A20) simulation suggests a conceptual problem when unresolved (implicit) and resolved (explicit) clouds coexist at the same grid through a deep layer, especially during the storm evolution period when each of the cumulus parameterization and explicit schemes can produce a significant amount of latent heating (see Fig. 3). This is because under such a situation the characteristic time scale of parameterized subgrid-scale convection may approach that of convection on the grid-scale and the implicit and explicit clouds can represent the essentially similar physical process (Molinari and Dudek, 1992). This problem might be less severe if the transition from subgrid-scale heating to grid-scale heating occurs rapidly. However, this is not the case in the present tropical cyclone model simulations because the transition period is for several days. Therefore, an approach using both cumulus parameterization and explicit method to represent convective processes in numerical models may be called a *pragmatic*

approach [This does not include the hybrid approach discussed in Molinari and Dudek (1992)].

Historically, precipitation observed in nature has been categorized into convective and stratiform (nonconvective) precipitation. According to this, in the large-scale numerical models the precipitation resulting from the subgrid-scale cumulus convection has been referred to as convective precipitation and that resulting from the grid-scale supersaturation stratiform precipitation. In the present tropical cyclone model with a 20 km horizontal resolution (for instance in the C20 simulation), this division of precipitation is valid during the early storm development when the model atmosphere is subsaturated and conditionally unstable (convective precipitation). However, this division is not valid in the eyewall region of the mature storm because in the model grid-scale heating is dominant there but in nature convective clouds are dominant there, although stratiform precipitation occupies over wider areas.

To investigate the effects of including a more accurate evaporation scheme on the storm development, two numerical experiments are conducted in which the experimental design of the model is the same as that in the B20 (C20) simulation except that the evaporation rate for liquid water in the subsaturated region is represented by

$$E_p = 134.5 \rho^{-0.325} \varepsilon q_l^{0.675} (q_{vs} - q_v) \quad (13)$$

with

$$\begin{aligned} \varepsilon = & 3.3 \times 10^{-5} - 4.75 \times 10^{-7} (p - 77.5) - \\ & 6.25 \times 10^{-9} (p - 77.5)^2 \end{aligned} \quad (14)$$

Here, ρ is in g/cm³ and p in centibar. This formula was used by Rosenthal (1978) to represent the evaporation rate for rain water in his axisymmetric tropical cyclone model.

Figure 4 shows the time evolution of the minimum surface pressure for the BN20 and CN20 cases (corresponding to the B20 and C20 cases, respectively). Similar to the previous result (Fig. 1), the minimum surface pressure in the CN20 simulation is slightly lower than that in the BN20 simulation during the early days of the time integration due to the parameterized latent heat release in the CN20 simulation. A detailed examination of the time evolution of the latent heating field for these two

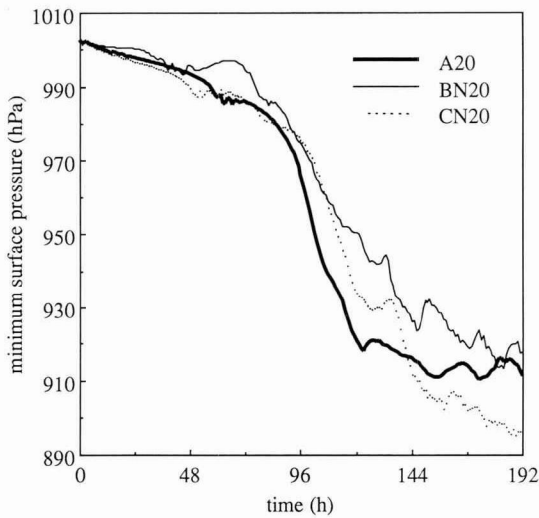


Fig. 4. The time evolution of the minimum surface pressure for the experiments with the explicit method (BN20) and the cumulus parameterization and explicit method (CN20) with an alternative representation of evaporation rate for liquid water. Also, the time evolution of the A20 experiment is plotted for comparison.

experiments reveals that the exaggerated cooling rates observed in the B20 and C20 simulations are considerably reduced with an inclusion of the more accurate scheme for treating evaporation rate for liquid water. However, the conceptual problem discussed above still arises in the CN20 simulation.

Figures 1 and 4 indicate that although the model storm evolution is somewhat sensitive to the treatment of convective processes, final storm intensities are not significantly different from each other. This is because the maximum intensity of tropical cyclones is strongly controlled by the sea surface temperature and an axisymmetric tropical cyclone model can produce a mature storm which is close to the theoretically estimated maximum possible intensity for a given sea surface temperature (Emanuel, 1986 and 1988; Rotunno and Emanuel, 1987; Baik *et al.*, 1990b).

Although a mature storm with theoretically estimated maximum possible intensity can be attained in an axisymmetric model given proper horizontal resolution and sufficient time, situation in nature is different. To get some insight into intensity degree that can be realized by tropical cyclones in nature and to get an implication to cumulus parameterization

scheme employed in tropical cyclone modeling, we define the ratio (R) as observed intensity of storm (OI) to potential intensity of storm (PI), that is,

$$R = \frac{OI}{PI} \quad (15)$$

and compute R for all the 1989 north Atlantic storms. If a storm achieves its potential intensity, R is equal to one. The theoretical work by Emanuel (1986 and 1988) indicated that an upper bound of tropical cyclone intensity (potential intensity) is determined by the local sea surface temperature and the mean outflow temperature of storm. During the 1989 north Atlantic storm season, storm activity was slightly above normal [4 tropical storms (Allison, Barry, Iris and Karen) and 7 hurricanes (Chantal, Dean, Erin, Felix, Gabrielle, Hugo and Jerry)] and strong Cape Verde type hurricanes (Gabrielle and Hugo) occurred. In this study, the potential intensities are calculated using the empirical potential intensity and the climatological sea surface temperature. An empirical function for the potential intensity based on the climatological sea surface temperature and maximum wind speed data (Merrill, 1988) is given by (DeMaria and Kaplan, 1991; Baik *et al.*, 1991a; DeMaria *et al.*, 1993)

$$PI = 38.04 \exp[0.21(T_s - 25)] \quad (16)$$

where PI is the potential intensity (m/s) and T_s the sea surface temperature (°C). The climatological sea surface temperature at the best track position is used to obtain PI . Maximum wind speed and best track data at 12 h intervals (00 Z and 12 Z) and climatological sea surface temperature data are archived from the Hurricane Research Division / Atlantic Oceanographic and Meteorological Laboratory / NOAA for R calculation.

The histogram showing the distribution of R for the 1989 north Atlantic storms is given in Fig. 5. Among the 142 available cases, the 20 cases for which the climatological sea surface temperature at the best track position is less than 25°C is eliminated from the calculation and the remaining 122 cases are considered. In R calculation, the maximum wind speed at any synoptic time is used for OI . This figure indicates that the 62 cases (about half of the total cases) have R values larger than 0.50 and the 9 cases have R values larger than 0.90 (~ 7% of the sample). Remember that the total 122 cases include

intensifying and decaying stages as well as mature stages of the storms.

Figure 6 shows the histogram of each storm versus R for which the life-time maximum wind speed for each storm is used for OI . If the archived life-time maximum wind speed at a specific synoptic time is equal to that at the next consecutive time, an average value of R for the two consecutive synoptic times is used for this figure. It is shown that hurricanes Erin,

Felix, Gabrielle and Hugo achieved almost their potential intensity during their life-time, while hurricane Dean achieved 80% of its potential intensity during its life-time. However, the other 6 storms attained their maximum intensities which are much weaker than their potential intensities (lower values of R). Figures 5 and 6 imply that environmental influences are as important as sea surface temperature in determining tropical cyclone intensity.

Evans (1991) investigated the relationship between the maximum sustained wind observed during the storm's life-time and the sea surface temperature over 5 ocean basins for the 20 year period. The results indicated that there is no obvious correlation between the storm's life-time maximum intensity and the sea surface temperature, suggesting that environmental influences play a major role. The vertical shear of horizontal wind (e.g., DeMaria *et al.*, 1993) and the reduction of sea surface temperature by oceanic mixing and upwelling induced by the storm circulation (e.g., Khain and Ginis, 1991) have negative influences on tropical cyclone intensification. The cumulus parameterization scheme employed in this study is constructed on the thermodynamic basis and does not include the large-scale dynamic influences on the subgrid-scale cumulus convection. Since the vertical shear of horizontal wind is an important factor in determining tropical cyclone intensity, further effort is needed to include vertical wind shear effects in the convective adjustment scheme (Betts, 1986) to better simulate tropical cyclones in a baroclinic zone and hence better understand the nature of tropical cyclones through three-dimensional numerical modeling studies.

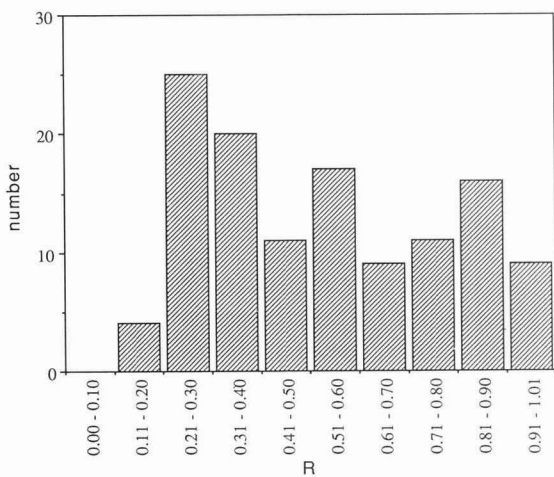


Fig. 5. Histogram for the distribution of R for the 1989 north Atlantic storms. In R calculation, the maximum wind speed at any synoptic time is used for OI .

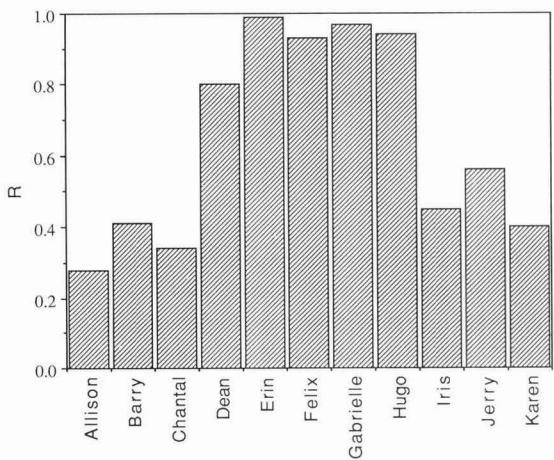


Fig. 6. Histogram for the distribution of R for each 1989 north Atlantic storm. In R calculation, the maximum wind speed during each storm's life-time is used for OI .

3.2 Inertial Stability Analysis During the Rapid Intensification Stage

In this subsection, the model output data from the simulation with the cumulus parameterization and simple method of removing grid-scale supersaturation (A20 experiment) are used to analyze the rapidly intensifying stage of the model storm and investigate the roles of inertial stability in the rapid intensification. Figure 7 shows the time evolution of the maximum wind speed at the lowest model level (level 15). The intensification rate of the model storm in terms of the maximum lowest level wind speed is

similar to that of the minimum surface pressure (A20 case in Fig. 1), that is, the storm develops slowly during the first 3 days, intensifies rapidly during the next 2 days and attains a mature state thereafter. The maximum vertical velocity and the maximum total latent heating rate plotted at 24 h intervals (Fig. 8) reflect similar storm development stages to Figs. 1 and 7. Based on Figs. 1, 7 and 8, we define a rapidly intensifying stage as the period between 72 h and 120 h for the subsequent analyses.

The central pressure drop for the period 72 h-96 h (denoted by R1, hereafter) is 20 hPa and for the period 96 h-120 h (denoted by R2, hereafter) it is 45 hPa (Fig. 1). Therefore, this simulated tropical cyclone belongs to the category of the rapidly intensifying typhoons defined by Holliday and Thompson (1979).

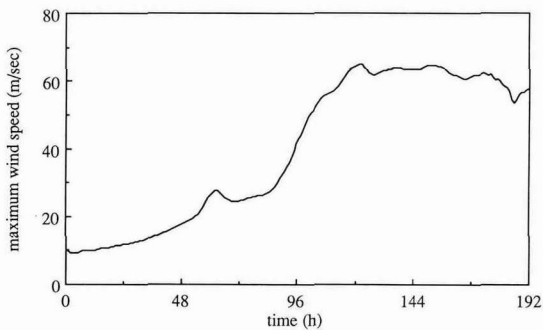


Fig. 7. The time evolution of the maximum wind speed at the lowest model level for the A20 experiment.

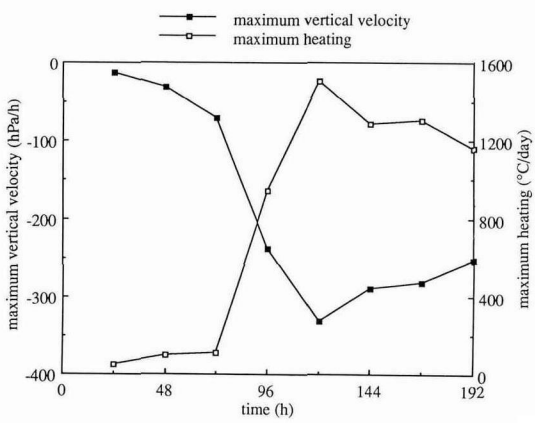


Fig. 8. The time evolution of the maximum vertical velocity and the maximum total latent heating for the A20 experiment.

The radial distribution of the surface pressure at 72, 96 and 120 hours is shown in Fig. 9. This figure indicates that the surface pressure drop during R2 is larger than that during R1 at all radii. Figure 10 shows the radial distribution of the tangential wind speed at 72, 96 and 120 hours at levels 3, 8 and 15 (representing upper, middle and lower troposphere, respectively). The time evolution of the vortex structure in terms of the tangential wind speed at level 15 indicates that inside about 250 km radius the maximum tangential wind moves inward and increases with larger change during R2 than during R1. On the other hand, the radial gradient of the tangential wind speed beyond that radius remains nearly-unchanged during the rapid intensification. At level 8, the vortex inside about 200 km radius also evolves more rapidly during R2 than during R1. At level 3, the cyclonic circulation strengthens near and inside the radius of the maximum wind with time and the anticyclonic circulation exists beyond 450 km radius at 72 h and 96 h and 490 km radius at 120 h. This figure also shows that at levels 3, 8 and 15 the radial gradient of the tangential wind speed inside the location of the maximum wind increases with time.

Inertial stability parameter is a measure of resistance to the horizontal displacement of an air parcel and can be expressed by (Schubert and Hack, 1982)

$$\sigma_i = \left(\frac{\partial v}{\partial r} + \frac{v}{r} + f \right) \left(\frac{2v}{r} + f \right) \quad (17)$$

where f is the Coriolis parameter. When the atmosphere becomes more inertially stable, an air

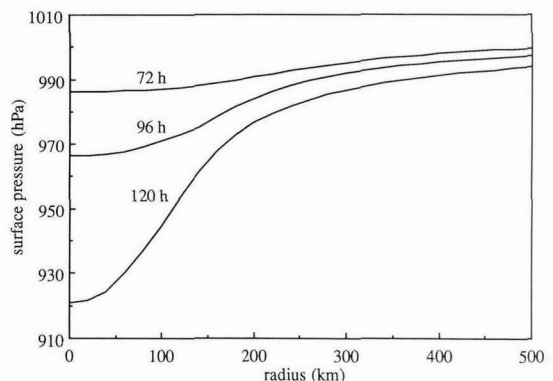


Fig. 9. The surface pressure as a function of radius at 72, 96 and 120 hours for the A20 experiment.

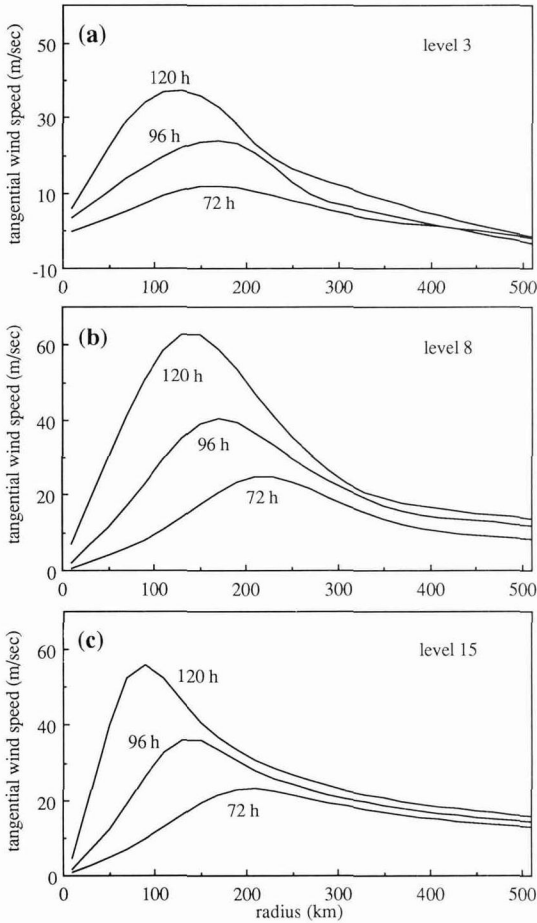


Fig. 10. The tangential wind speed as a function of radius at 72, 96 and 120 hours at levels (a) 3, (b) 8 and (c) 15 for the A20 experiment.

parcel flowing in the radial direction experiences more resistance and the transverse circulation weakens. For the same diabatic heat source, increasing inertial stability leads to weaker vertical motion and decreased adiabatic cooling in the ascending branch of transverse circulation. Hence, a smaller fraction of the diabatic heating is used to compensate for the adiabatic cooling and a larger fraction is used to warm the air column. Thus, the diabatic heating is used more efficiently as the inertial stability increases. In the linear CISK (Conditional Instability of the Second Kind) theory, which is only valid for the tropical cyclone during the very early stage, the inertial stability can be approximated by f^2 and the adiabatic cooling rate in the ascending region

is as large as the cumulus heating rate. Therefore, the efficiency to warm the atmosphere is low. However, when also considering the effects of the $(\partial v / \partial r + v/r)$ and $2v/r$ terms in (17), which become more important during deepening stage, the inertial stability and the efficiency can grow in a nonlinear feedback mechanism (Schubert and Hack, 1982). Another possible effect of inertial stability is that as it becomes larger the relative vorticity increases so the boundary layer pumping is enhanced because the frictionally induced vertical velocity at the top of the Ekman layer is proportional to the relative vorticity of the surface wind (Charney and Eliassen, 1964). Therefore, the transverse circulation associated with boundary layer pumping increases (remark given by Emanuel in the footnote of the paper by Schubert and Hack, 1982).

To examine overall features of the vortex structure, the radius-height cross sections of the tangential wind speed at 48, 72, 96, 120 and 144 hours are plotted in Fig. 11. At 48 h, the cyclonic circulation occurs throughout the entire atmosphere inside the radius of 270 km, and the anticyclonic circulation exists beyond that radius in the upper portion of the atmosphere and extends outward. During the next 24 hours, the cyclonic circulation strengthens a little and the maximum cyclonic circulation zone moves inward. At 72 h, two separate zones with high tangential wind speed exist; one is located at level 5 ($\sigma \sim 0.21$) at ~ 170 km radius and the other at level 14 ($\sigma \sim 0.95$) at ~ 210 km radius. During R1 (R2), the cyclonic circulation strengthens rapidly and the radius of the maximum wind at the lowest model level reduces by 60 (40) km. During the period 120 h–144 h, the overall features of the tangential wind field remains quasi-steady.

Figure 12 shows the radius-height cross section of the inertial stability at 48, 72, 96, 120 and 144 hours. A common feature at 48, 96, 120 and 144 hours is that the most inertially stable region is located near just inside the radius of the maximum wind in the lower troposphere, where both the tangential wind speed and the radial gradient of the tangential wind speed (positive) are large. At 72 h, two separate regions of high inertial stability are seen in the lower troposphere and at \sim level 5. Both regions are located near just inside of the two separate maximum wind zone (see tangential wind field at 72 h in Fig. 11). However, as the maximum wind zone confines within the lower troposphere with time, the inertially stable zone

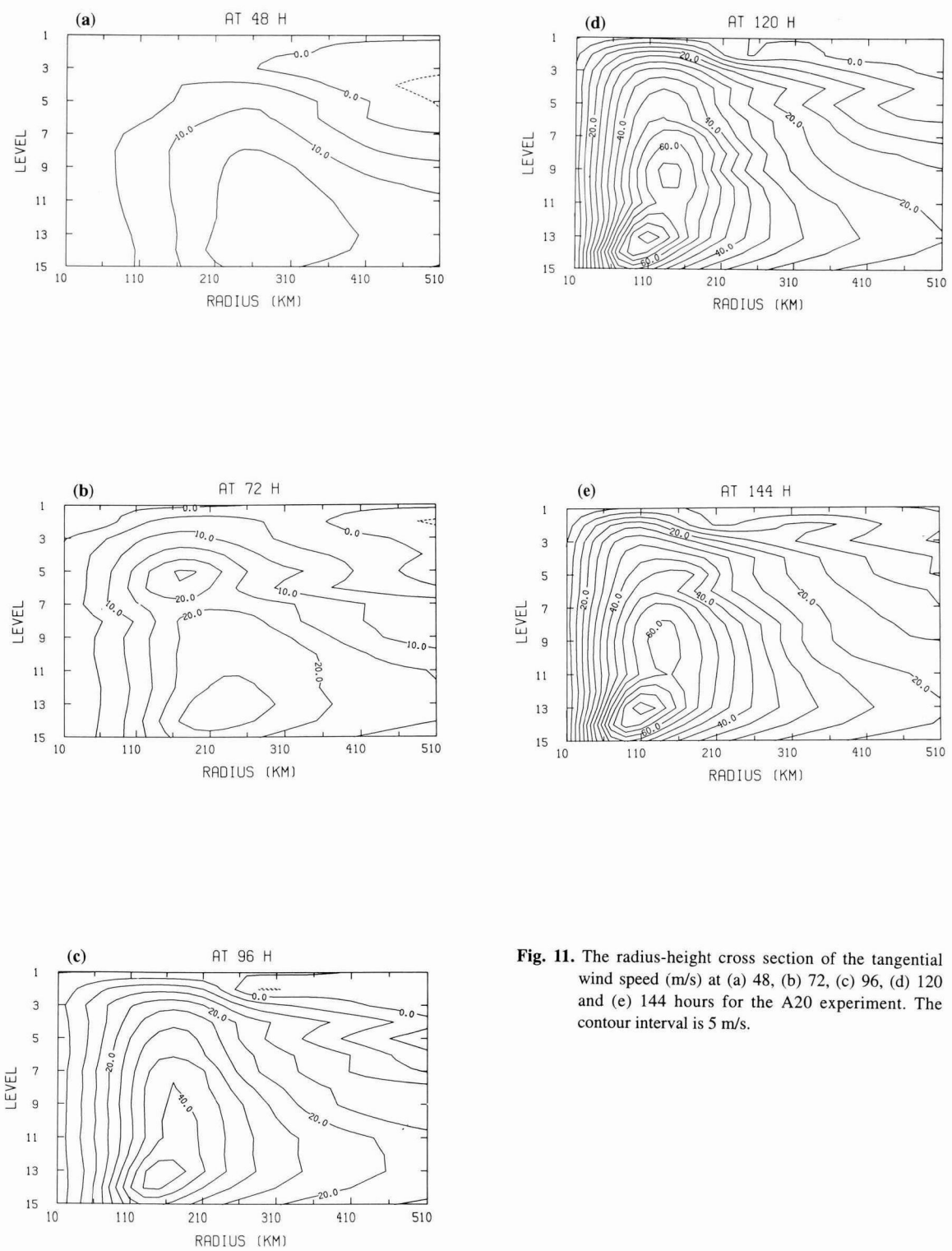


Fig. 11. The radius-height cross section of the tangential wind speed (m/s) at (a) 48, (b) 72, (c) 96, (d) 120 and (e) 144 hours for the A20 experiment. The contour interval is 5 m/s.

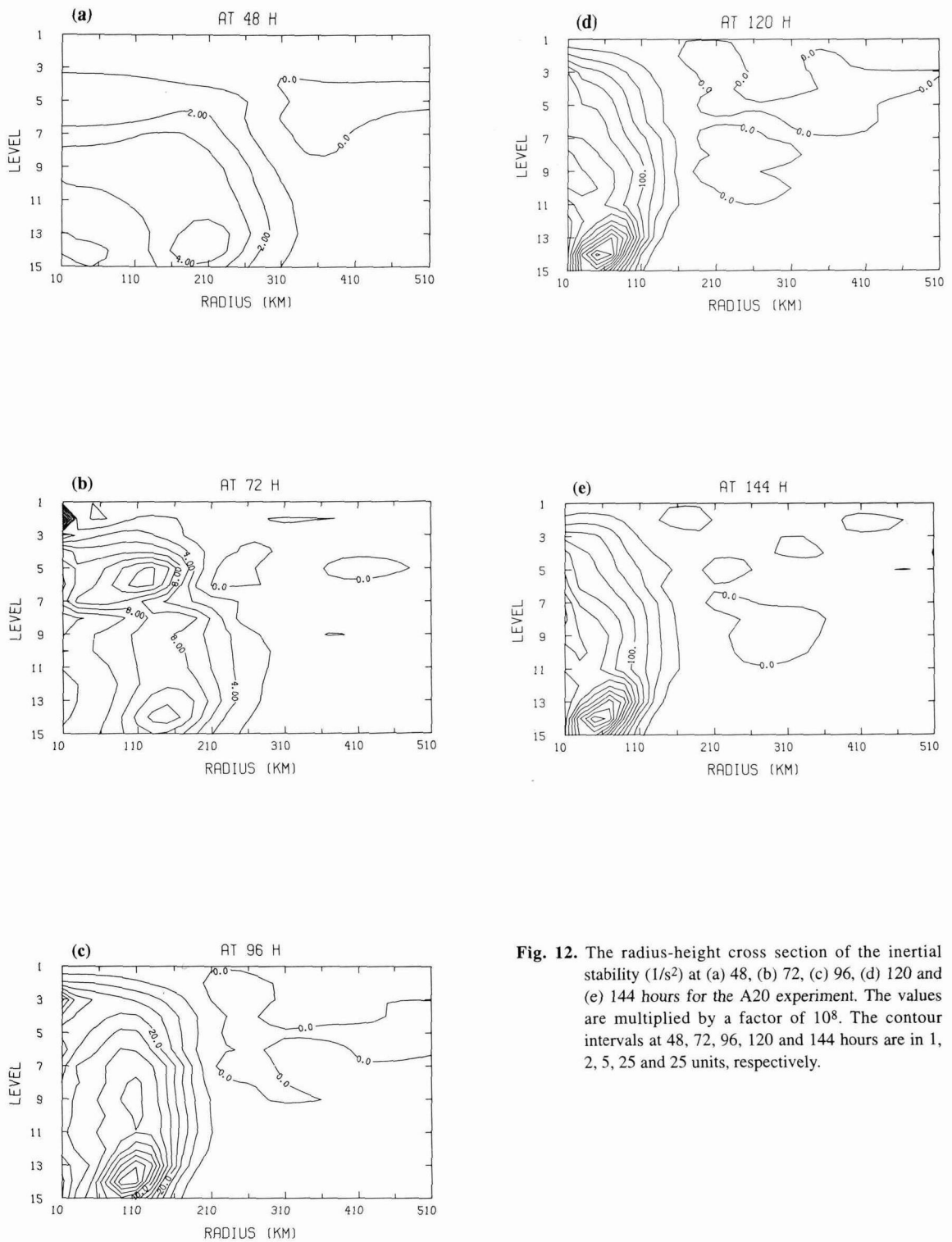


Fig. 12. The radius-height cross section of the inertial stability ($1/s^2$) at (a) 48, (b) 72, (c) 96, (d) 120 and (e) 144 hours for the A20 experiment. The values are multiplied by a factor of 10^8 . The contour intervals at 48, 72, 96, 120 and 144 hours are in 1, 2, 5, 25 and 25 units, respectively.

located at ~level 5 becomes much less intense than that in the lower troposphere. During the rapid intensification, the inertially stable region in the lower troposphere becomes much more inertially stable and moves inward. At 120 h, the maximum zone of inertial stability in the lower troposphere is located near 50 km radius and the maximum value is considerably larger than that at 96 h. During the period 120 h-144 h, the inertial stability field remains nearly-unchanged inside 150 km radius. Figure 12 also shows inertially unstable regions in the middle and upper portions of the atmosphere in a broad elongated pattern (48, 96 and 120 hours) or a patched pattern (72 and 144 hours).

Based on Fig. 12, we state the relation between inertial stability and rapid intensification of the storm as follows. The most inertially stable region exists just inside the radius of the maximum wind in the lower troposphere, where both the tangential wind speed and the radial gradient of the tangential wind speed are large. An air parcel moving towards the storm center in the lower troposphere has a large resistance to horizontal motion as it approaches the inertially stable region. Hence, the parcel is deflected upward and convection is confined to the area just outside the most inertially stable region. The heating efficiency is higher in the inertially stable region. The atmosphere becomes warmer and the surface pressure falls down. The tangential wind speed increases more efficiently and accordingly the inertial stability increases. Therefore, the storm can develop rapidly through a positive feedback mechanism between increasing inertial stability and increasing heating efficiency.

Figure 12 indicates that near and inside the radius of the maximum wind the lower troposphere is more inertially stable than the middle and upper troposphere and the outflow region can become inertially unstable. This implies that when a tropical cyclone in nature interacts with its environment (e.g., approaching upper-level troughs in the midlatitudes or upper-level cold lows in the low latitudes), the upper-level environmental forcing is much more permeable to affecting tropical cyclone intensity than the low-level environmental forcing because of strong resistance to horizontal motion in the high inertial stability region.

4. Conclusions

For the range of horizontal model resolution over which either implicit or explicit convective scheme can simulate tropical cyclones well, it is unclear which approach outperforms the other in tropical cyclone models. A method of including both implicit method (cumulus parameterization) and explicit method for this range of model resolution can provide some advantages, but with a conceptual ambiguity when the implicit and explicit clouds coexist at the same horizontal grid location through a deep layer.

Based on the theoretical work by Schubert and Hack (1982) and the numerical model simulation, it was emphasized that a nonlinear positive feedback between the increasing inertial stability, especially near and inside the radius of the maximum wind in the lower troposphere, and the increasing heating efficiency to warm the atmosphere can play an important role in the rapid intensification of the storm. A recent observational study (personal communication with Edward Rodgers, 1993) indicates that the correlation between the satellite-derived latent heating and the subsequent intensity change becomes higher as the storms become more intense. One possible explanation for this is that more intense storms have higher inertial stability around the region of the maximum wind and the higher heating efficiency, hence possibly resulting in noticeable positive intensity changes. Further study to combine the satellite-derived rainfall rates (latent heating) with the aircraft-measured wind data is needed to observationally document the roles of inertial stability in the tropical cyclone intensification.

Acknowledgments

The authors would like to thank Mark DeMaria and Edward Rodgers for providing valuable comments on this study and Jae-Sang Jung for helping preparation of the manuscript. This research was partly supported by the Korea Science and Engineering Foundation under contract NO. 91-07-00-11.

References

- Anthes, R.A., 1977: Hurricane model experiments with a new cumulus parameterization scheme. *Mon. Wea. Rev.*, 105, 287-300.
- _____, 1982: *Tropical Cyclones: Their Evolution, Structure and Effects*. Meteor. Monogr., No. 41., Amer. Meteor. Soc., 208 pp.
- Baik, J.-J., M. DeMaria and S. Raman, 1990a: Tropical cyclone simulations with the Betts convective adjustment scheme. Part I: Model description and control simulation. *Mon. Wea. Rev.*, 118, 513-528.
- _____, _____ and _____, 1990b: Tropical cyclone simulations with the Betts convective adjustment scheme. Part II: Sensitivity experiments. *Mon. Wea. Rev.*, 118, 529- 541.
- _____, _____ and _____, 1991a: Observational evidence for upper-tropospheric asymmetric eddy momentum forcing and subsequent hurricane intensity change. *19th Conference on Hurricanes and Tropical Meteorology*, Miami, Amer. Meteor. Soc., 478-481.
- _____, _____ and _____, 1991b: Tropical cyclone simulations with the Betts convective adjustment scheme. Part III: Comparisons with the Kuo convective parameterization. *Mon. Wea. Rev.*, 119, 2889-2899.
- Betts, A.K., 1986: A new convective adjustment scheme. Part I: Observational and theoretical basis. *Quart. J. Roy. Meteor. Soc.*, 112, 677-691.
- Charney, J.G., and A. Eliassen, 1964: On the growth of the hurricane depression. *J. Atmos. Sci.*, 21, 68-75.
- DeMaria, M., and J. Kaplan, 1991: A statistical model for predicting tropical cyclone intensity change. *19th Conference on Hurricanes and Tropical Meteorology*, Miami, Amer. Meteor. Soc., 521-526.
- _____, J.-J. Baik and J. Kaplan, 1993: Upper-level eddy angular momentum fluxes and tropical cyclone intensity change. *J. Atmos. Sci.*, 50, 1133-1147.
- Emanuel, K.A., 1986: An air-sea interaction theory for tropical cyclones. Part I: Steady-state maintenance. *J. Atmos. Sci.*, 43, 585-604.
- _____, 1988: The maximum intensity of hurricanes. *J. Atmos. Sci.*, 45, 1143-1155.
- Evans, J.L., 1991: Tropical cyclone sensitivity to sea surface temperatures. *19th Conference on Hurricanes and Tropical Meteorology*, Miami, Amer. Meteor. Soc., 471-474.
- Gray, W.M., E. Ruprecht and R. Phelps, 1975: Relative humidity in tropical weather systems. *Mon. Wea. Rev.*, 103, 685-690.
- Hack, J.J., and W.H. Schubert, 1980: *The role of convective-scale processes in tropical cyclone development*. Dept. of Atmos. Sci. Pap. No. 330, Colorado State University, Ft. Collins, CO, 206 pp.
- _____, and W.H. Schubert, 1981: Lateral boundary conditions for tropical cyclone models. *Mon. Wea. Rev.*, 109, 1404-1420.
- Holliday, C.R., and A.H. Thompson, 1979: Climatological characteristics of rapidly intensifying typhoons. *Mon. Wea. Rev.*, 107, 1022-1034.
- Jones, R.W., 1980: A three-dimensional tropical cyclone model with release of latent heat by the resolvable scales. *J. Atmos. Sci.*, 37, 930-938.
- Kasahara, A., 1961: A numerical experiment on the development of a tropical cyclone. *J. Meteor.*, 18, 259-282.
- Khain, A., and I. Ginis, 1991: The mutual response of a moving tropical cyclone and the ocean. *Contrib. Atmos. Phys.*, 64, 125-142.
- Kurihara, Y., 1975: Budget analysis of a tropical cyclone simulated in an axisymmetric numerical model. *J. Atmos. Sci.*, 32, 25-59.
- Liu, J.Y., and H.D. Orville, 1969: Numerical modeling of precipitation and cloud shadow effects on mountain-induced cumuli. *J. Atmos. Sci.*, 26, 1283-1298.
- Merrill, R.T., 1988: Environmental influences on hurricane intensification. *J. Atmos. Sci.*, 45, 1678-1687.
- Molinari, J., and M. Dudek, 1986: Implicit versus explicit convective heating in numerical weather prediction models. *Mon. Wea. Rev.*, 114, 1822-1831.
- _____, and _____, 1992: Parameterization of convective precipitation in mesoscale numerical models: A critical review. *Mon. Wea. Rev.*, 120, 326-344.
- Ooyama, K., 1964: A dynamical model for the study of tropical cyclone development. *Geofis. Int.*, 4, 187-198.
- _____, 1982: Conceptual evolution of the theory and modeling of the tropical cyclone. *J. Meteor. Soc. Japan*, 60, 369-380.
- Rosenthal, S.L., 1978: Numerical simulation of tropical cyclone development with latent heat release by the resolvable scales I: Model description and preliminary results. *J. Atmos. Sci.*, 35, 258-271.
- Rotunno, R., and K.A. Emanuel, 1987: An air-sea interaction theory for tropical cyclones. Part II: Evolutionary study using a nonhydrostatic axisymmetric numerical model. *J. Atmos. Sci.*, 44, 542-561.
- Schubert, W.H., and J.J. Hack, 1982: Inertial stability and tropical cyclone development. *J. Atmos. Sci.*, 39, 1687-1697.
- Seitter, K.L., 1986: A numerical study of atmospheric density current motion including the effects of condensation. *J. Atmos. Sci.*, 43, 3068-3076.
- Weatherford, C., 1987: Typhoon structural evolution. *17th Conference on Hurricanes and Tropical Meteorology*, Miami, Amer. Meteor. Soc., 337-340.

- Willoughby, H.E., H.-L. Jin, S.L. Lord and J.M. Piotrowicz, 1984: Hurricane structure and evolution as simulated by an axisymmetric, nonhydrostatic numerical model. *J. Atmos. Sci.*, 41, 1169-1186.
- Yamasaki, M., 1977: A preliminary experiment of the tropical cyclone without parameterizing the effects of cumulus convection. *J. Meteor. Soc. Japan*, 55, 11-31.
- Zhang, D.-L., 1988: The effect of parameterized ice microphysics on the simulation of vortex circulation with a mesoscale hydrostatic model. *Tellus*, 41A, 132-147.